

Thickness and Growth Temperature Dependence of Structure and Magnetism in FePt Thin Films

Michael F. Toney[a],* Wen-Yaung Lee[b], Jonathan A. Hedstrom and Andrew Kellock

IBM Almaden Research Center

IBM Research Division

650 Harry Road

San Jose, Ca 95120

(Dated: March 25, 2003)

Abstract

We describe structural and magnetic measurements of polycrystalline, $L1_0$ chemical-ordered Fe(55-60)Pt(45-40) films as a function of film thickness (from 3 to 13 nm) and growth temperature (270 - 370 °C). With increasing film thickness, the coercivity increases from about 1 kOe up to 11 kOe (growth at 400°C), while for increasing growth temperature, the coercivity grows from 0.2 to 6 kOe for 4.3 nm thick films and 1.6 to 10 kOe for 8.5 nm thick films. There is a strong, nearly linear correlation between coercivity and the extent of $L1_0$ chemical order. In all the films there is a mixture of $L1_0$ and chemically disordered, fcc phases. The grain size in the $L1_0$ phase increases with both film thickness and growth temperature (increasing chemical order), while in the fcc phase the grain size remains nearly constant and is smaller than in the $L1_0$ phase. The films all contain twins and stacking faults. The relationship between the coercivity and the film structure is discussed and we give a possible mechanism for the lack of chemical order in the very thin films (lack of nucleation sites for the $L1_0$ phase).

PACS numbers: 75.50.SS, 75.50.Vv, 68.55.Jk, 61.10.Nz

*Electronic address: mftoney@slac.stanford.edu

I. INTRODUCTION

The materials used as future media for magnetic recording at high areal densities will have higher magnetic anisotropy than the CoPtCrB alloys presently used in recording. The high magnetic anisotropy is necessary to insure thermal stability in future media, which will have small grain size. While several alternative high anisotropy materials are attractive candidates [1], the chemically ordered $L1_0$ alloys, such as equicomposition FePt, FePd and CoPt, are particularly appealing and thin films of these materials have received a great deal of attention in the past decade. In these future media, the areal moment density of the media ($M_r T$, where M_r is the remnant magnetization and T is the media thickness) will also be smaller than in present CoPtCrB media (due to the scaling required to increase areal density). Since the magnetic moment in these $L1_0$ alloys is significantly larger than the present CoPtCrB alloys (about 3-4 times larger) [1], $L1_0$ films used in recording will be physically quite thin (≈ 3 -5 nm). Hence, it is important to understand how film thickness affects the magnetic and structural properties of FePt alloy films, which is the purpose of this publication.

Thin films of FePt and related $L1_0$ alloys have been studied since the early 1980s [2, 3], but there was renewed interest beginning about 10 years ago [4, 5], which was mostly driven by the potential use of these materials as recording media or for magneto-optical applications. Thermodynamically, below $1300^\circ C$ equicomposition FePt forms a chemically ordered $L1_0$ structure, where there are alternating atomic planes of Pt and Fe along the c -axis [6]. The chemical ordering drives a tetragonal distortion in the unit cell, and in bulk FePt, $c/a = 0.96$ [6], where c is the lattice parameter along the chemical order direction and a is the lattice parameter orthogonal to this. However, in thin films the formation of the $L1_0$ phase requires either annealing or deposition at elevated temperatures ($\gtrsim 400^\circ C$). Films deposited near room temperature adopt a disordered face-centered cubic (fcc) structure. Since annealing and high temperature deposition can lead to large grains (unsuitable for magnetic recording), there have been efforts to reduce the grain size by either doping to lower the annealing/deposition temperatures [7-9] or forming nanophase composite films [10].

In bulk FePt and related hard $L1_0$ alloys, it has been reported that the high coercivity in these alloys is due to the formation of a finely dispersed mixture of fcc and $L1_0$ phases

[11] or, alternatively, to the presence of planar defects (anti-phase boundaries (APB) and/or twin boundaries [12, 13]), which act as pinning sites. However, it is not clear which of these mechanisms (or some combination of them) is most important. In thin films, however, the coercivity mechanism is likely different than in bulk materials, since the grains are small enough that they are single domain and since the dependence of coercivity on composition differs in films and bulk materials [14]. There have been several papers discussing the coercivity mechanism in $L1_0$ thin films, and these have suggested several possible sources for the coercivity in these films, including pinning at the boundaries between fcc and $L1_0$ phases [15, 16] or at APBs [15] or twin boundaries [14]. Since, in thin films, much of this work is in infancy, the dominant mechanism contributing to the coercivity is still unclear.

As mentioned above, quite thin FePt films will be required for magnetic recording. To date, there has been only a little work related to the effect of film thickness on the magnetic properties of FePt [5, 17]. These show a drop in coercivity with decreasing film thickness, but no structural data have been reported. Equicomposition MnPt and MnNi also form chemically ordered $L1_0$ phases, which are antiferromagnetic and are used in spin valve sensors. For these materials, it is observed that with decreasing MnPt or MnNi thickness, there is a drastic loss in chemical order [18, 19].

In this paper, we describe the changes in magnetism and structure in polycrystalline FePt films (on 1 nm Pt seedlayers) as a function of thickness (from 3 to 13 nm) and, to a lesser extent, on growth temperature (270 - 370 °C). We find that the coercivity decreases with film thickness and annealing temperature and is strongly correlated with the extent of $L1_0$ chemical order. In partly chemically ordered films, the $L1_0$ phase coexists with the fcc phase (two phase material). With increasing chemical order (either with increasing thickness or annealing temperature), the FePt grain size in the $L1_0$ phase increases, but the grain size in the fcc phase does not change. For all film thicknesses, there are twins and stacking faults, but the relationship between these and the coercivity is not clear. Finally, we suggest that the mechanism limiting chemical ordering in the thin films is nucleation of the $L1_0$ phase, which we believe is also important for $L1_0$ MnPt and MnNi [18].

II. EXPERIMENTAL ASPECTS

The FePt films were deposited on glass or Si substrates in a DC magnetron sputtering system having a base pressure of around 2×10^{-8} Torr at a substrate temperature (T_s) of 22°C and 1×10^{-7} Torr at a T_s of 400°C . Both $\text{Fe}_{50}\text{Pt}_{50}$ and $\text{Fe}_{55}\text{Pt}_{45}$ targets were used to deposit these films and films were grown on 1 nm Pt seedlayers. The substrate temperature was calibrated under the actual deposition conditions with a thermocouple bonded to the glass or Si substrates. The magnetic properties of these films were obtained at ambient temperature using a commercial vibrating sample magnetometer (VSM) with a maximum magnetic field of 1.6 kOe. The film composition and thickness were determined by Rutherford backscattering spectroscopy (RBS) and particle induced X-ray emission (PIXE).

Most of the diffraction measurements were performed at the National Synchrotron Light Source beamline X20C with an energy of about 10 keV using a Ge detector to eliminate the Fe X-ray fluorescence. The diffracted beam was analyzed with 1 milliradian (mrad) Soller slits and the acceptance perpendicular to the scattering plane was about 14 mrad. A variety of X-ray diffraction data were collected to determine the extent of chemical order, lattice parameters, extent of the (111) texture and grain size. Much of the data were collected using a grazing incidence geometry where the incident and diffracted X-ray beams are at small (about 2 degrees (deg)) angles to the film surface. Such a geometry minimizes the background scattering from the glass substrates and measures diffraction planes perpendicular to the surface. Measurements on the film texture were obtained with a lab-based source using Cu $K\alpha$ radiation.

III. MAGNETIC RESULTS

Figure 1 shows the thickness dependence of the longitudinal coercivity (H_c) and saturation magnetization (M_s) for deposition at 400°C . With increasing thickness, H_c increases quickly and then plateaus, while M_s decreases and plateaus. Note that since M_s is measured in a 1.6 kOe field, the FePt films may not be fully saturated. The thickness behavior for H_c is qualitatively similar to that reported for FePt films deposited at room temperature and then annealed [5, 17]. As shown below, the dependence of H_c on thickness (Fig. 1(a)) results from the strong increase in chemical order with increasing film thickness. This also

explains the magnetization behavior, since the disordered phase has a higher moment than the chemically ordered phase [20].

Figure 2 shows the dependence of the H_c and M_s on growth temperature for 4.3 and 8.5 nm thick FePt films. These results are qualitatively similar to the growth temperature dependence reported before for FePt [21–24] and other $L1_0$ alloys [25]. These data are consistent with an increase in chemical order with growth temperature, as shown below.

We note that there was some anisotropy in the VSM loops of the FePt films (perpendicular compared with longitudinal), but we did not carefully investigate this because the primary focus of this work is the longitudinal behavior of the FePt films.

IV. STRUCTURAL RESULTS

Before we discuss the results of the structural characterization, it is important to describe the states of $L1_0$ chemical order that exist in these FePt films. In a binary alloy, such as FePt, the extent of chemical order is typically quantified by the order parameter:

$$S = r_{Pt} + r_{Fe} - 1 = (r_{Pt} - x_{Pt})/y_{Fe} = (r_{Fe} - x_{Fe})/y_{Pt}. \quad (1)$$

Here x_{Pt} and x_{Fe} are the atom fractions of Fe and Pt, respectively; r_{Pt} and r_{Fe} are the fraction of Fe and Pt sites occupied by the correct atom in the $L1_0$ structure; and y_{Pt} and y_{Fe} are the fraction of correct Fe and Pt sites, 0.5 in for the $L1_0$ phase [6, 26, 27]. When the chemical order is perfect, all the Fe-sites are occupied by Fe atoms and Pt-sites by Pt atoms and $S=1$, while for complete chemical disorder, all sites are equally occupied by Fe and Pt and $S=0$. For partial chemical order, S is proportional to the number of atoms on correct sites ($r_{Fe} + r_{Pt}$). From the definition of S above, perfect order is achievable only for exact stoichiometry. For other compositions, the maximum S depends on composition with $S_{max} = 1 - 2x$, where x is the compositional deviation from 0.5 [21]. S_{max} is marked with arrows on figures showing chemical order.

The discussion above is applicable to homogeneous materials, but a material can be inhomogeneous, consisting of regions that have high chemical order and regions that are nearly disordered (e.g., a two-phase system). This distinction between the microstructures suggests that an additional factor is needed to quantify chemical order in inhomogeneous materials. This is the volume fraction of the film that is chemically ordered, which we call

f_o . For inhomogeneous materials, we can then distinguish (and, in principle, measure) f_o , S_{order} (S in the chemically ordered regions), and S_{ave} (the volume average S). The latter, however, is just $S_{ave} = f_o \times S_{order}$ [6].

Figure 3 shows grazing incidence diffraction data for a series of FePt with thicknesses from 3.3 nm to 13 nm. There are several structural changes with FePt thickness. First, the thinnest film is only weakly chemically ordered as evidenced by the weak (110) peak (near $Q=2.3 \text{ \AA}^{-1}$) and unsplit (220) peak at $Q=4.6 \text{ \AA}^{-1}$. Second, with increasing film thickness, the $L1_0$ superlattice peaks appear strongly and the fcc (220) peak splits into the $L1_0$ (220) and (202) peaks; this signals the presence of significant chemical order. Third, focusing on the region of Fig. 3 near (220) peak near $Q=4.6 \text{ \AA}^{-1}$, it is apparent in the 4-10 nm films that there are three diffraction peaks. This has also been verified by peak fitting; three peaks (fcc(220) and $L1_0$ (202) and (220)) are needed to adequately fit the data. This shows that there is two phase coexistence between fcc and $L1_0$ FePt phases in these films. Last, the diffraction peaks sharpen with increasing thickness, which means the average lateral grain size increases with film thickness.

Before showing the quantitative results of the extent of chemical order in these films, it is useful to briefly describe how this is determined. We use the ratio of the integrated intensities of the $L1_0$ (110) and (220) peaks to calculate S_{order} [6, 26]. The ordered-volume fraction, f_o , is determined from the fitted intensities of the fcc(220) and $L1_0$ (202) and (220) peaks as the ratio of the $L1_0$ peaks to the sum of the three peak intensities. The volume averaged chemical order, S_{ave} , is the product of S_{order} and f_o . As a check and to improve the accuracy of the analysis, S_{ave} was also determined from the ratio of the $L1_0$ (110) peak to the sum of the fcc(220) and $L1_0$ (202) and (220) peaks.

Figure 4 summarizes the thickness dependence of chemical order for films grown at 400° C. Recalling that the FePt films are two phase, this shows that the ordered portion of the films is highly chemically ordered with S_{order} about 0.9, independent of thickness. With increasing thickness, the chemically ordered fraction f_o increases and hence the average S_{ave} also increases. Above about 10 nm, highly ordered films ($S_{ave} = 0.8$ with $S_{max} = 0.9$) are obtained at 400° C. Figure 5 shows the temperature dependence of chemical order for the nominally 4.2 and 8.5 nm films. As with the thickness series, S_{order} is independent of temperature and constant at about 0.8. The chemically ordered fraction increases with growth temperature leading to increases in S_{ave} and modestly ordered films are obtained for

growth near 360° C.

The data presented above show that for these films the microstructure is two phase with highly chemically ordered regions $S_{order} = 0.8 - 0.9$ and chemically disordered (fcc) regions. This two-phase microstructure is commonly, probably ubiquitously, observed in $L1_0$ sputter deposited thin films that are either annealed or grown at elevated temperatures [6, 15, 16, 18, 28]. This is probably a result of the formation of the $L1_0$ chemically ordered phase by nucleation and growth, which in turn is a consequence of the first order nature of the $L1_0$ to fcc phase transition (i.e., there is coexistence of both ordered and disordered phases at the phase transition temperature). In contrast, it appears that FePt films grown at elevated temperatures by ultra-high vacuum evaporation are not two phase, but are single phase and homogeneous, even for partial chemical order [21].

Figure 6 shows the correlation between coercivity and chemical order, measured by S_{ave} . As is apparent, there is a strong, approximately linear, correlation between these. While Fig. 6 compares H_c and S_{ave} , an equally strong correlation would be obtained between H_c and f_o , since S_{order} is 0.8-0.9 in all the films. This strong correlation between coercivity and chemical order is similar to that observed before in FePt [15, 22] and FePt-MgO [23] films grown at different temperatures as well as $L1_0$ CoPt [15]. The origin of this dependence is the strong dependence of the magnetic anisotropy on chemical order [29–31].

The in-plane lattice parameters for these FePt films have been calculated from the diffraction peak positions. For both the $L1_0$ and fcc components of the films, there is a slight decrease in the lattice parameters as a function of film thickness (about 0.2% from 3.3 to 13 nm) for films grown at 400° C. In the 4.2 and 8.4 nm films, the lattice parameters are essentially independent of growth temperature. The average values of the lattice parameters are $a=3.86$ Å and $c=3.74$ Å for the $L1_0$ components and $a=3.82$ Å for the fcc. This contrasts with $a=3.85$ Å and $c=3.71$ Å for bulk $L1_0$ $Fe_{50}Pt_{50}$. Hence, the lattice parameters of the films are slightly larger than bulk, which is likely caused by film growth. Furthermore, the c/a ratios are slightly larger in the films ($c/a=0.970$) than in bulk ($c/a=0.963$), which has some implications on the magnetic anisotropy [31, 32]. Large c/a ratios (closer to unity) in films have been observed by others in FePt [33] and other $L1_0$ films [6, 34]. This is probably a manifestation of the film growth, since most of the films in this and other studies had $S \approx 1$. In some studies of $L1_0$ materials, the c/a ratio has been used as a measure of S [35]. The large c/a ratio that we and others observe suggest that this approach is likely to yield

unreliable results.

As mentioned above, the diffraction peaks become sharper with increasing FePt thickness (Fig. 3), which indicates the lateral grain size in the films increases. To quantify this, we have determined the physical crystallite size from the diffraction peak widths using the method of integral breadths [26]. Figure 8(a) and (b) show the results of this analysis for the thickness and temperature series, respectively, for both the chemically ordered (filled squares) and disordered (open squares) parts of the films. As is evident (Fig. 8(a)), the crystallite size of the transformed ($L1_0$) phase increases significantly with increasing film thickness. In contrast, the crystallite size of the fcc or untransformed phase is much smaller than the $L1_0$ phase and does not increase much with thickness. As expected (Fig. 8(b)), the crystallite size of the $L1_0$ phase also increases with increasing growth temperature; again, the fcc crystallites are smaller than for the $L1_0$ phase and they do not grow with temperature. The growth dependence of particle size in the $L1_0$ component of the films (Fig. 8) is consistent with that observed previously for growth temperature [28] and film thickness (for significantly thicker films) [36]. For $L1_0$ ordered NiMn and MnPt in sputter deposited and subsequently annealed spin valves, the $L1_0$ crystallites are significantly larger than the fcc crystallites [18]. We believe that this is due to the formation of the $L1_0$ phase by nucleation and growth; once this phase forms, it grows quickly (since it is thermodynamically stable), while the untransformed fcc part of the film does not grow significantly. Since most of the $L1_0$ materials of interest in magnetism form by nucleation and growth [6], this suggests that the difference in crystallite sizes is common to these $L1_0$ thin films grown by sputter deposition.

Pole figure measurements of the films showed that all the films had a dominant (111) texture along with about 20% of the film untextured or isotropic. For the growth temperature series, there was a small decrease in the (111) rocking curve width with increasing growth temperature (dropping from about 13 deg to about 10 deg). For the thickness series, the rocking curve widths were independent of the film thickness (for 3.3 to 13 nm) to within the error bars. This preferred orientation probably causes the anisotropic magnetic properties mentioned above.

Various types of planar or extended crystalline defects are present in most materials and it has been suggested [12, 13] that these influence the coercivity, although the nature of the defects affecting H_c is unclear. As is evident in Fig. 3, the (200) and (002) diffraction

peaks in the films considered here are broader than the (111) peaks, which results from the presence of stacking faults in the FePt films. Since the positions of the (200) and (002) peaks are not shifted from those expected based on the lattice parameters, these stacking faults are not deformation faults [26], but are growth faults ($\{111\}$ twins). From the widths of these peaks, we can determine the fault density or, equivalently, the average spacing between faults [26]. This fault spacing is shown in Fig. 8 for both the thickness (8(a)) and temperature (8(b)) series. The growth fault spacing increases (fewer growth faults) as both the film thickness and growth temperature increases. This is reasonable, since the crystalline quality of the FePt films (measured, for example, by crystallite size and extent of chemical order) improves with both increasing thickness and growth temperature.

We also observe that the (001) peaks are somewhat broader than the (002) peaks, which is a manifestation of antiphase domains in the chemically ordered portions of the FePt films [6, 26]. However, due to the strong background scattering from the glass substrates in the region near the (001) peak, it is difficult to accurately determine the (001) peak width. Hence, we do not have good quantitative data on these defects and only note that they are present in the film with a density slightly less than the growth faults.

V. DISCUSSION

As mentioned in the introduction, the dominant mechanism contributing to the coercivity in $L1_0$ thin films is not well established; both the boundaries between fcc and $L1_0$ phases [15, 16] and planar defects (APBs and twins [14, 15]) have been postulated as possible pinning sites. The data for our films show the following: there is a strong correlation between S and H_c (Fig. 6); in our mostly highly ordered films, there is still some fcc phase (Fig. 4); there are both twin faults (or boundaries) and APBs in all our films (Fig. 8 and discussion above). The strong dependence of H_c on S merely results from the dependence of the magnetic anisotropy on chemical order [29–31]. While hardly definitive, the presence of twin boundaries and APBs and the small concentration of fcc phase suggests that the planar defects are important in determining the coercivity. However, more work is needed (where the defect levels are carefully varied) to firmly establish this.

Other work (see Introduction) has shown that both MnPt and NiMn exhibit a similar dependence of the chemical order on film thickness with the chemical order developing as

film thickness increases and the chemically ordered phase forming by nucleation and growth and coexisting with a disordered fcc phase for some thicknesses [18, 19]. This suggests a common mechanism that slows the $L1_0$ ordering for the very thin films in these materials. We expect that the transformation rate of the fcc phase into the $L1_0$ phase is limited by nucleation, since the grains in the $L1_0$ phase are large while those of the fcc phase are small and do not depend on film thickness or growth temperature. This then suggests that the lack of chemical order in the thin films is due to a lack of nucleation sites, since for a given concentration of nucleation sites, thinner films will have fewer sites. This suggests that by increasing the number of nucleation sites (smaller initial grain size) one could increase the fcc-to- $L1_0$ transformation rate. Because thinner films develop less $L1_0$ order, surfaces and interfaces are not nucleation sites.

The $L1_0$ FePt films described here have high enough coercivity for a thermally stable recording medium at advanced recording densities. However, the grain size is too large for low noise media, which is a direct result of the high growth temperatures needed to form the $L1_0$, high anisotropy phase. Suitable media can possibly be obtained by either lowering the growth or annealing temperatures (through surfactants) [7], forming nanophase composite films [10], or through growth on different seedlayers [37].

VI. SUMMARY AND CONCLUSIONS

We have described the thickness and growth temperature dependence of the magnetism and structure in polycrystalline FePt films. The coercivity increases with increasing film thickness and annealing temperature and is strongly correlated with the $L1_0$ chemical order. The films are two phase with the $L1_0$ phase coexisting with the fcc phase. The FePt grain size in the $L1_0$ phase increases with increasing chemical order, but the fcc phase grain size is small and independent of film thickness or growth temperature. For all film thicknesses, there are twins, stacking faults and antiphase domain boundaries.

Our data suggest that the lack of chemical order in the thin films is due to a lack of nucleation sites for the $L1_0$ phase, consistent with observations on the related MnPt and MnNi systems [18]. It appears that planar defects (twin boundaries and APBs) are important in determining the coercivity, although more work is needed to confirm this. For FePt thin films to be useful as a recording media, methods of limiting grain size are needed.

Acknowledgments

We thank Kelly Hannibal and Ben Burrill for assistance with the data analysis. This research was carried out (in part) at the National Synchrotron Light Source, Brookhaven National Laboratory, which is supported by the U.S. Department of Energy, Division of Materials Sciences and Division of Chemical Sciences, under Contract No. DE-AC02-98CH10886.

-
- [a] Permanent Address: Stanford Synchrotron Radiation Laboratory, Stanford Linear Accelerator Center, Menlo Park, CA 94025
- [b] Permanent Address: Hitachi Global Storage Technologies, 5600 Cottle Road, San Jose, CA 95193
- [1] D. Weller *et al.*, IEEE Trans. Magn. **36**, 10 (2000).
- [2] J. A. Aboaf, S. R. Herd, and E. Klokhholm, IEEE Trans. Magn. **19**, 1514 (1983).
- [3] J. A. Aboaf, T. R. McGuire, S. R. Herd, and E. Klokhholm, IEEE Trans. Magn. **20**, 1642 (1984).
- [4] B. M. Lairson, M. R. Visokay, R. Sinclair, and B. M. Clemens, Appl. Phys. Lett. **62**, 639 (1993).
- [5] K. R. Coffey, M. A. Parker, and J. K. Howard, IEEE Trans. Magn. **31**, 2737 (1995).
- [6] A. Cebollada, R. F. C. Farrow, and M. F. Toney, in *Magnetic Nanostructures*, edited by H. S. Nalwa (American Scientific, Stevenson Ranch, Ca, 2002), p. 93.
- [7] S.-R. Lee, S. Yang, Y. K. Kim, and J. G. Na, Appl. Phys. Lett. **78**, 4001 (2001).
- [8] S.-R. Lee, S. Yang, Y. K. Kim, and J. G. Na, J. Appl. Phys. **91**, 6857 (2002).
- [9] T. Maeda *et al.*, Appl. Phys. Lett. **80**, 2147 (2002).
- [10] G. P. Luo and D. J. Sellmyer, Appl. Phys. Lett. **75**, 3162 (1999).
- [11] H. Okumura, W. A. Soffa, T. J. Klemmer, and J. A. Barnard, IEEE Trans. Magn. **34**, 1015 (1998).
- [12] B. Zhang and W. A. Soffa, Phys. Stat. Sol. **131**, 707 (1992).
- [13] T. J. Klemmer *et al.*, Scripta. Metall. Mater. **33**, 1793 (1995).
- [14] M. H. Hong, K. Hono, and M. Watanabe, J. Appl. Phys. **84**, 4403 (1998).
- [15] R. A. Ristau *et al.*, J. Appl. Phys. **86**, 4527 (1999).
- [16] S. Jeong, Y.-N. Hsu, D. E. Laughlin, and M. E. McHenry, IEEE Trans. Magn. **37**, 1299 (2001).
- [17] S.-Y. Bae, K.-H. Shin, J.-Y. Jeong, and J.-G. Kim, J. Appl. Phys. **87**, 6953 (2000).
- [18] M. F. Toney, M. G. Samant, T. Lin, and D. Mauri, Appl. Phys. Lett. **81**, 4565 (2002).
- [19] W. Y. Lee *et al.*, IEEE Trans. Magn. **38**, 3536 (2002).
- [20] A. Z. Men'shikov, V. A. K. Yu A. Dorofeyev, and S. K. Sidorov, Fiz. Met. Metalloved. **38**, 505 (1974).

- [21] R. F. C. Farrow *et al.*, Appl. Phys. Lett. **69**, 1166 (1996).
- [22] J.-C. Shih, H.-H. Hsiao, J.-L. Tsai, and T.-S. Chin, IEEE Trans. Magn. **37**, 1280 (2001).
- [23] T. Suzuki and K. Ouchi, IEEE Trans. Magn. **37**, 1283 (2001).
- [24] S. Jeong *et al.*, J. Appl. Phys. **91**, 6863 (2002).
- [25] P. Caro, A. Cebollada, F. Briones, and M. F. Toney, J. Cryst. Growth **187**, 426 (1998).
- [26] B. E. Warren, *X-ray Diffraction* (Addison-Wesley, Reading, MA, 1969).
- [27] F. C. Nix and W. Shockley, Rev. Mod. Phys. **10**, 1 (1938).
- [28] K. Barmak *et al.*, J. Appl. Phys. **79**, 5330 (1996).
- [29] S. Mitani *et al.*, J. Magn. Magn. Mater. **148**, 163 (1995).
- [30] P. Kamp *et al.*, Phys. Rev. B **59**, 1105 (1999).
- [31] S. S. A. Razee *et al.*, Phys. Rev. B **64**, 4411 (2001).
- [32] A. Sakuma, J. Phys. Soc. Japan **63**, 3053 (1994).
- [33] Y.-N. Hsu, S. Jeong, D. E. Laughlin, and D. N. Lambeth, J. Appl. Phys. **89**, 7068 (2001).
- [34] M. F. Toney, unpublished.
- [35] M. Chen and D. E. Nikles, J. Appl. Phys. **91**, 8477 (2002).
- [36] H. H. Hsiao, R. N. Panda, J. C. Shih, and T. S. Chin, J. Appl. Phys. **91**, 3145 (2002).
- [37] J.-U. Thiele, M. E. Best, M. F. Toney, and D. Weller, IEEE Trans. Magn. **37**, 1271 (2001).

Figure Captions

Figure 1. H_c (a) and M_s at 1.6 kOe (b) vs film thickness for growth at $T=400^\circ$ C.

Figure 2. H_c (a) and M_s at 1.6 kOe (b) vs growth temperature for $t=4.3$ (filled symbols) and 8.5 nm (open symbols) thick FePt films.

Figure 3. Grazing incidence X-ray diffraction data as a function of FePt film thickness. The data are offset for clarity. In this geometry, we are measuring planes perpendicular to the sample normal. Q is the scattering vector which has a magnitude $Q = (4\pi/\lambda)\sin\theta$, where λ is the X-ray wavelength. The $L1_0$ (001) and (110) superlattice peaks are at 1.7 and 2.3 \AA^{-1} , respectively. The broad background scattering near 1.8 and 4.5 \AA^{-1} is due to the glass substrate.

Figure 4. Dependence of chemical order on FePt film thickness for films grown at 400° C. (a) Average S . (b) S in the chemically ordered regions of the film. (c) Fraction of the film that is chemically ordered. The arrows mark the maximum achievable chemical order (due to deviation from exact 1:1 stoichiometry).

Figure 5. Dependence of chemical order on growth temperature for 4.3 and 8.5 nm FePt thick films (closed and open symbols, respectively). (a) Average S . (b) S in the chemically ordered regions of the film. (c) Fraction of the film that is chemically ordered. The arrows mark the maximum achievable chemical order.

Figure 6. Correlation between coercivity (H_c) and chemical order (S_{ave}). Data are for all the films considered in this study.

Figure 7. Average crystallite size determined using the integral breadth method. Filled symbols are for the $L1_0$ component of the films, while open symbols are for the fcc component. The lines are guides. (a) Crystallite size as a function of film thickness. (b) Crystallite size as a function of growth temperature. Circles and squares are data for 4.3 and 8.5 nm FePt thick films, respectively, while the solid and dashed lines are guides for these film thicknesses.

Figure 8. Average stacking fault spacing. (a) Growth fault spacing as a function of FePt film thickness for growth at 400° C. (a) Growth fault spacing as a function of FePt growth temperature for 4.3 nm (open squares) and 8.5 nm (filled circles).

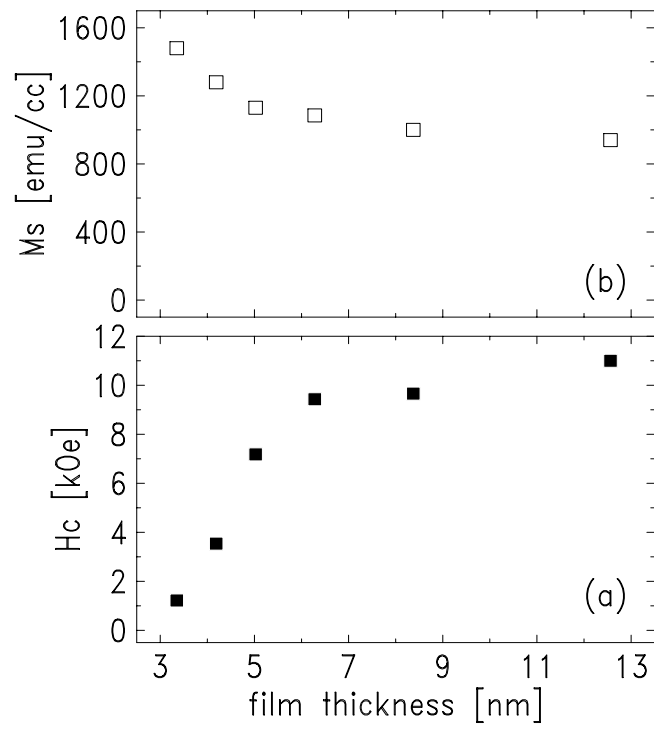


FIG. 1: Toney et al., JR02-3531

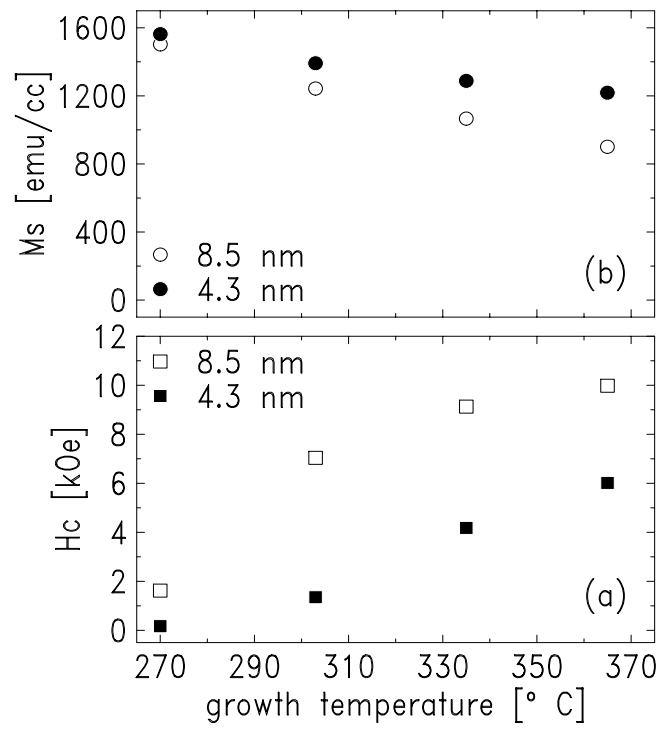


FIG. 2: Toney et al., JR02-3531

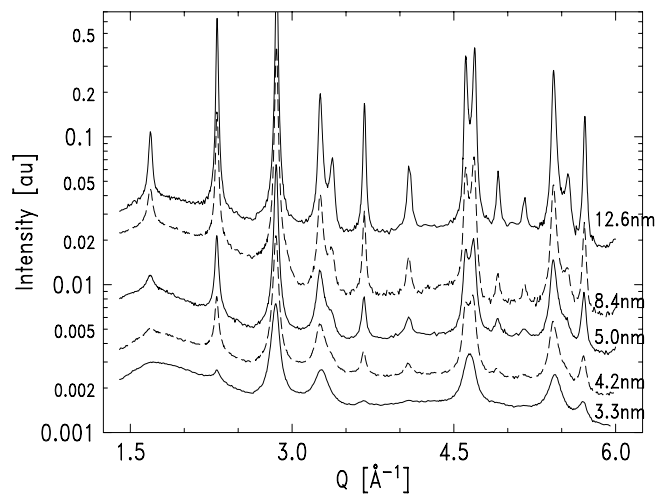


FIG. 3: Toney et al., JR02-3531

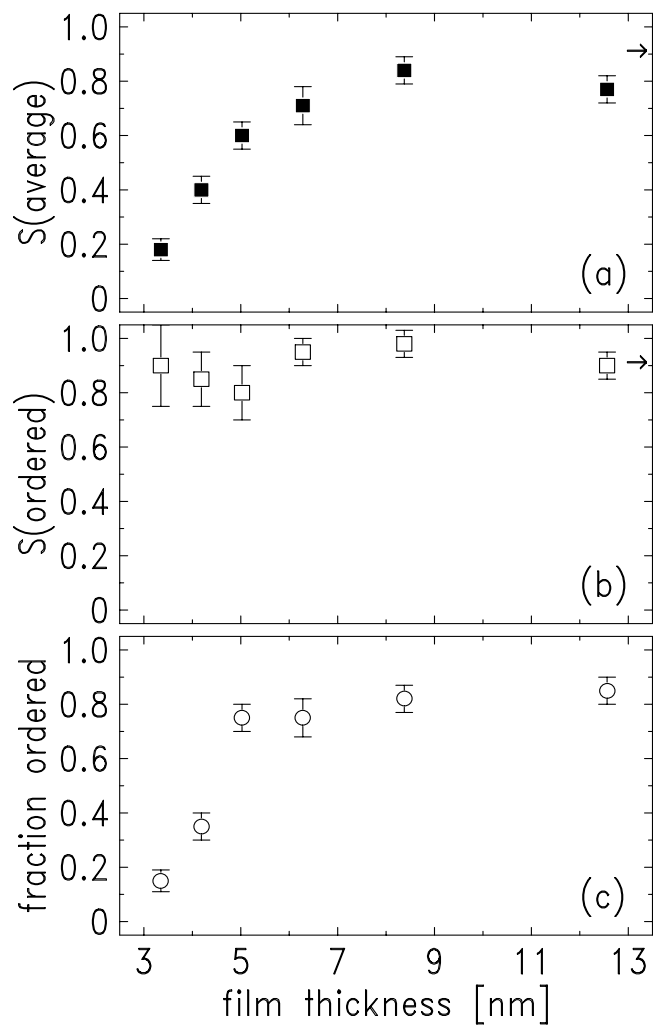


FIG. 4: Toney et al., JR02-3531

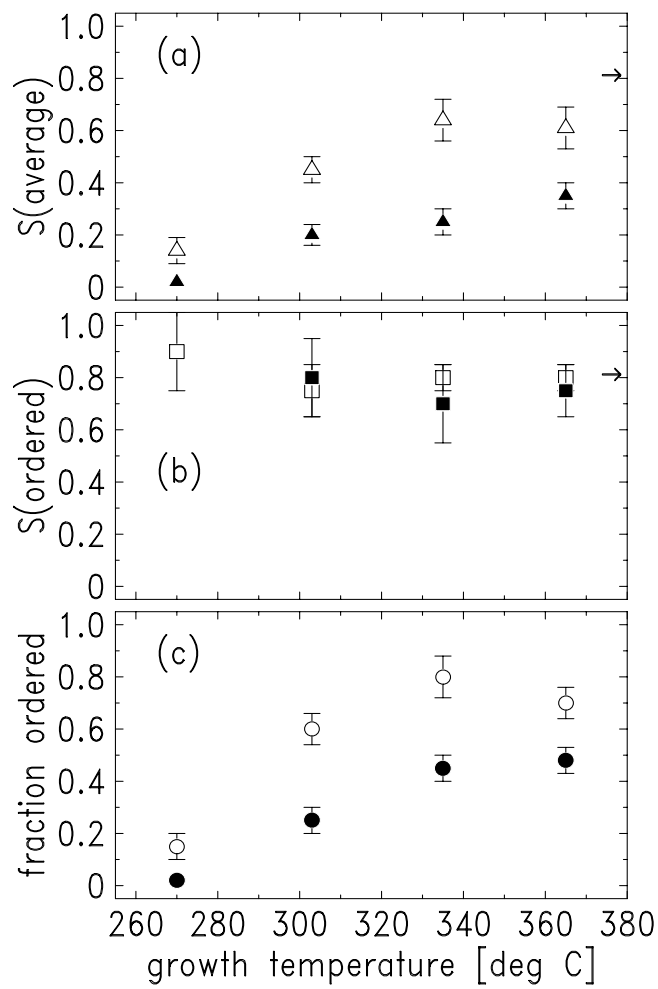


FIG. 5: Toney et al., JR02-3531

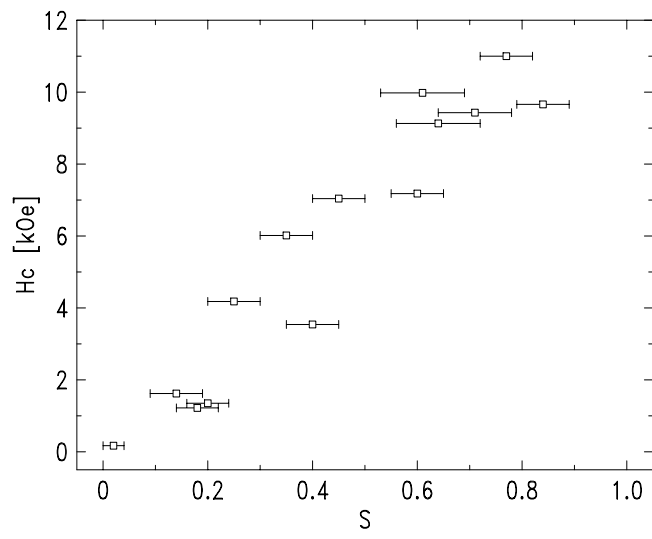


FIG. 6: Toney et al., JR02-3531

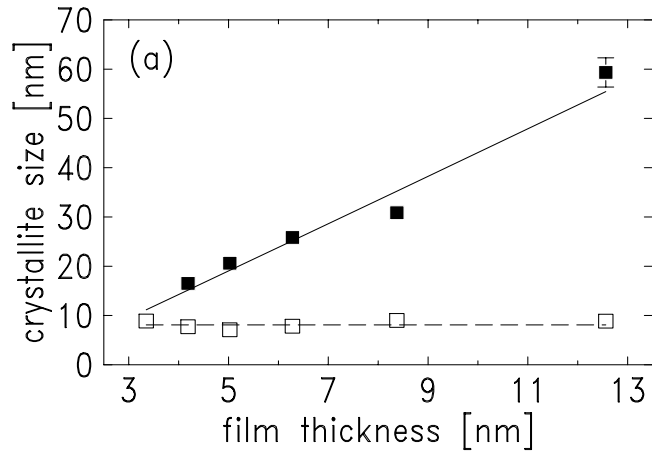
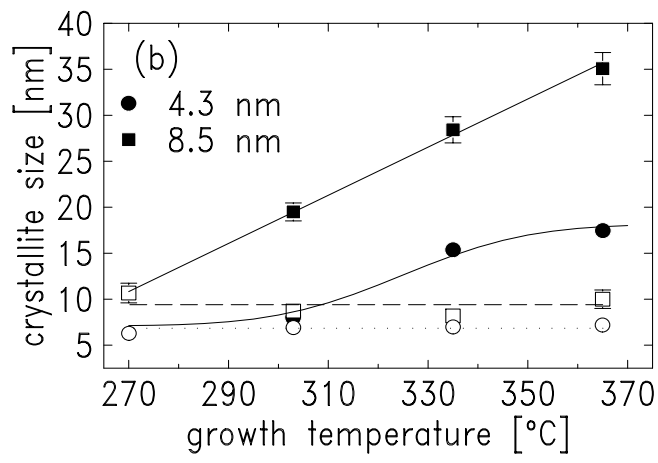


FIG. 7: Toney et al., JR02-3531

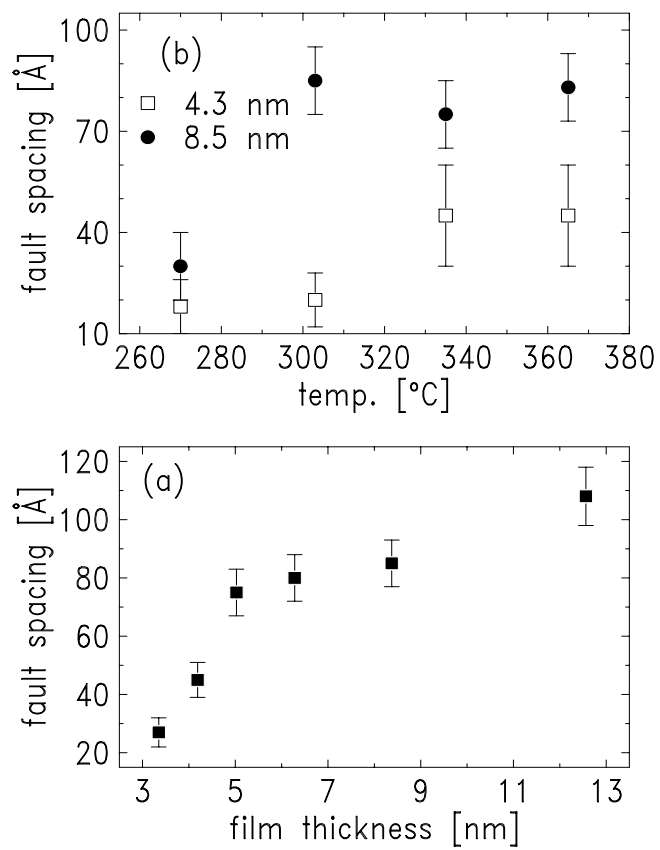


FIG. 8: Toney et al., JR02-3531